J. Water Environ. Nanotechnol., 6(3): 241-251 Summer 2021

ORIGINAL RESEARCH PAPER

Green Synthesis and Characterization of Copper Oxide Nanoparticles-Reduced Graphene Oxide Nanocomposites for Facile Electrochemical Oxidation of Ponceau 4R and Alizarin Red Dyes in Aqueous Medium

R.Vijayalakshmi [1*], S.Kanchana[1], J.Santhanalakshmi [2]

[1] Department of Chemistry, Quaid E Millath Government College for Women, Annasalai,Chennai 600 002,Tamil Nadu, India

[2] Department of Physical Chemistry,University of Madras, Maraimalai Campus, Chennai – 600 025 (Retd.), India

Received: 2021-05-10 Accepted: 2021-06-25 Published: 2021-07-01

ABSTRACT

Copper oxide nanoparticles are prepared to adopt the green synthesis route by using Aloe vera plant extract instead of synthetic and polymeric stabilizing agents in mild alkaline aqueous conditions. The synthesized CuO nanoparticles (CuO NPs) are characterized by Powder XRD and HR-TEM measurements. Using the as-synthesized CuO NPs and reduced graphene oxide (rGO), nanocomposites comprising CuO NPs- rGO are prepared by hydrothermal and ultrasonic methods. Nanocomposites are characterized using Powder XRD, HR-TEM, and FE-SEM data. The fabricated CuO NPs-rGO nanocomposites are coated onto glassy carbon electrode (GCE) for facile detection and electro-oxidation of water-polluting dyes such as the Ponceau 4R (P4R) and Alizarin Red (AR) using cyclic voltammetry. Electrooxidation of the dyes occurred at appreciably lower oxidation potentials like 0.45 V and 0.6 V for P4R and AR respectively along with the decoloration of the dyes. The absorbance of the analyte dye solutions is measured at intervals of time of the progress of electro oxidations. The overall first-order rate coefficient values for dye degradations are found out from absorbance time variance data. The results indicate that CuO NPs-rGO nanocomposites decorated GCE acted as an efficient electrode surface for sensing and degradation applications for the chosen dye solutions. P4R azo dye degradation response was found to be better than AR anthraquinone dyes.

Keywords: *CuO nanoparticles, reduced graphene oxide nanocomposites, Electrochemical oxidation of Ponceau 4R and Alizarin Red.*

How to cite this article

Vijayalakshmi R., Kanchana S, Santhanalakshmi J. Green Synthesis and Characterization of Copper Oxide Nanoparticles-Reduced Graphene Oxide Nanocomposites for Facile Electrochemical Oxidation of Ponceau 4R and Alizarin Red Dyes in Aqueous Medium. J. Water Environ. Nanotechnol., 2021; 6(3): 241-251.

DOI: 10.22090/jwent.2021.03.005

INTRODUCTION

The release of industrial effluents from textile dyeing, foodstuffs, soft beverages, cosmetics, drugs, paper, and plastic goods manufacturing units leaked, into vast natural water resources causes serious concern on the quality of water consumed by humans, aquatic life forms, and crops [1]. Eco–deadlier aspects are on the increase when intensely colored dye polluted wastewaters are consumed and enhanced due to the complex aromatic nucleus containing organic structures showing appreciable stability and slow degradation pathways. Even, some of the dye pollutants have been found to impart carcinogenic and mutagenic effects [2]. Henceforth detoxification and cleaning up of polluted water bodies are essentials and pose major challenges to environmental management

* Corresponding Author Email: *vijiradha68@gmail.com*

technologists [3]. The field of nanoscience offers numerous advanced nanomaterials possessing unique and enhanced chemical and physical properties that could be applied in wastewater treatments [4 -7]. Nanocomposites with organic and inorganic hybrid properties may be chosen to catalyze the mineralization of dyes in an eco-friendlier mechanism [8-12]. Generally, nanocomposites comprising metal or metal oxide nanoparticles bound onto carbon scaffolds possess multifunctionality that is exploited in sensing, catalytic, electron transfer, selective substrate-binding, etc applications in current science[13-22]. Among the class of synergetic carbon supports graphene, graphene oxide (GO) and reduced graphene oxide (rGO) systems are popular and widely used for deposition of metal and metal oxide nanoparticles producing large surface area to mass ratio values [23-27]. The nanomaterial rGO exhibits graphene-like properties along with oxygen functionalization on the surface which assists strong metal oxide nanoparticle bindings. Additionally, rGO can be synthesized by adopting eco-friendlier methods from cheap and abundant graphite material. The oxygen-rich functionalization in the rGO sheet aids its deposition onto electrode material like GCE. Construction of rGO nanocomposites with CuO NPs is expected to yield nanostructures which are compatible with glassy carbon electrodes having improved electrochemical properties compared to any other forms of carbonaceous nanomaterials. Also, literature reports imply CuO NPs possess significant characteristics such as cost-effectiveness electro stability, easy fabrication from the copper salt precursor, and having a low bandgap 2.0 eV that help in the remediation of eco-contaminants in industrial wastewaters [28] effectively. CuO nanoparticles find numerous applications as a catalyst, semiconductors, chelating or binding agent for complex organic substrates, etc [29-31]. In this work, CuO NPs are prepared via a green synthetic route by using Aloe vera plant extract as the stabilizing agent, instead of synthetic polymeric agents. In the green synthesis of CuO NPs the biomolecules found in plant extract act as the source of electrons for the metal oxide formations in the nano size, showing some advantages such as cost-effectiveness, good stability, safety, and easy operations[32-36]. The reported procedure involving copper salt precursor in mild alkaline aqueous medium and 40^0C thermostated solvent medium which are set in eco-friendlier conditions are only adopted [37]. The as-synthesized CuO NPs are size characterized from powder XRD and HR-TEM measurements. The CuO NPs are found to be spherical and showing a size range of 15±2.0 nm.

GO was prepared to adopt a green synthesis route with graphite powder and eco-friendlier mild process conditions which are extended to rGO formations also. Here, earlier reported procedures are adopted with minor modifications [38, 39]. CuO NPs are deposited onto rGO resulting in CuO NPs–rGO nanocomposites and the same are characterized using powder XRD, HRTEM, and FESEM measurements. Utilization of the fabricated nanocomposites find applications towards the modification of electrodic surfaces, imparting higher conductivity, substrate sensitivity, high surface area to mass ratio values, lowering of oxidation or reduction working potentials thus lowering the energy consumption, and robust towards the solution hydrothermal operational conditions with mild temperature and pressure values [40,41]. To confirm these aspects in this work, the CuO NPs–rGO nanocomposites are coated onto glassy carbon electrode (GCE) showing better chemical activity due to larger electrode surface area and higher electrocatalytic activity with high sensitivity, selectivity, and effective quantification [42]. Using this CuO-rGO modified GCE electrode, the electro-oxidation studies on the two widely used dyes, one of which is Ponceau 4R (P4R) (or) 2 hydroxy-1-(4-sulfonate-1-napthylazo)-6,8-naphthalene disulfonate trisodium ($C_{20}H_{11}N_2Na_3O_{10}S_3$) an azo dye with λ_{max} = 505nm are attempted. Its chemical structure has been represented in (Fig.1a), P4R has been profusely used in food, beverage, textile, paper, and cosmetic industries due to the intense coloration, lower price, water solubility, and high stability [43-45]. Another dye system, Alizarin Red (AR) or 1,2-dihydroxy-9,10-anthraquinone-3-sulfonic acid ($C_{14}H_7NaO_7S$) an anthraquinone dye with λ_{max} = 425nm was selected. Its chemical structure is given in (Fig.1b). AR is widely used in the textile industry, engineering, and gene expression studies. The fused ring structure of these dyes makes them lowly non-biodegradable and chemically stable [46-48],. Therefore prolonged consumption of P4 R and AR polluted water increases the intake concentration within the life systems which brings hazardous effects like carcinogenetic, Xenotoxicity, and retardation in the development

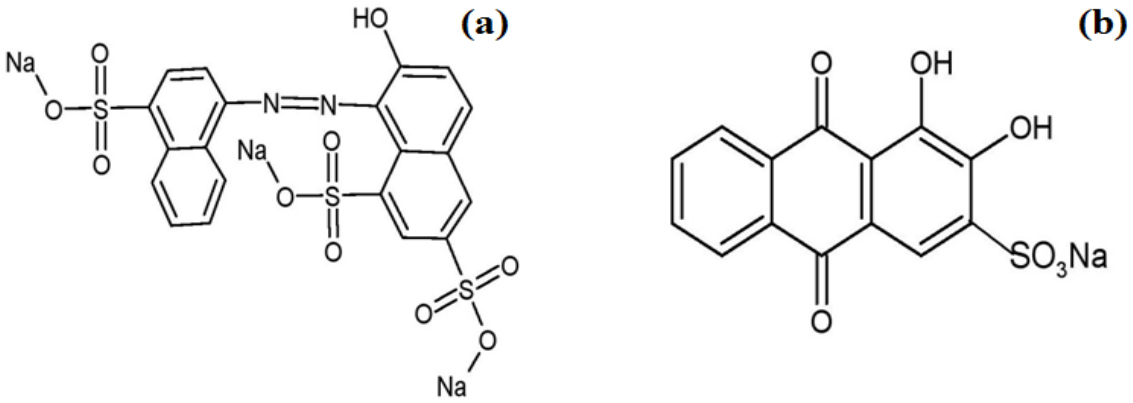

Fig. 1. (a). Molecular structure of Ponceau 4R and (b). Alizarin red.

of life forms [49]. In this work, the degradation of these dyes is followed by cyclic voltammetry with time variance on electro-oxidation scans. During electro oxidations, the dye analyte was found to be decolorized. The choice of electro-oxidation of dyes, confirms an eco-friendlier way of treatment of dye polluted water sources and also as dye sensors in an aqueous medium. In this work, during the progress of electro-decoloration of the dyes, concomitant visible spectra are run out on the samples drawn out at intervals of time. Time of completion of dye degradation was known from the oxidation peak values I_{pa} tracing zero and the absorbance values approaching zero in the visible spectra. From the absorbance variation with time data, the kinetic plots for overall rate coefficient value determinations are made. The results arrived from electro oxidations fall in agreement with those of the absorbance - time variance data. The novelty and implications of the results of this work expose that the CuO NPs–rGO nanocomposites are efficient electrocatalysts for the facile degradations of dyes in eco-friendlier pathways.

The main novelty of this work:

· Green synthesis of CuO nanoparticles using aloe vera plant extract as stabilizing agent resulting in average particle size 15 ± 2nm was achieved

· Nanocomposites comprising CuO nanop-articles and reduced graphite oxide was prepared from graphite precursor and mild enviro- friendlier experimental conditions

· CuO NPs -rGO oxide nanocomposites modified glassy carbon electrode was successfully designed and employed in the electrooxidation of the two dyes, Ponceau 4R and Alizarin Red analyte solutions.

· Using concomitant spectral absorbance variations with time measurements pseudo-first-order rate coefficient values of the dye degradations are determined and found out to be agreeable with those from electro oxidation results.

· The optimized electrooxidations are well suited for the azo dye Ponceau 4R mineralization which occurs in higher extents than anthraquinone Alizarin Red mineralizations.

EXPERIMENTAL

Chemicals

$Cu(NO_3)_2$ hydrated, NaOH pellets, graphite powder with particle size <50μm, 98% sulphuric acid, potassium permanganate, potassium nitrate, potassium chloride were procured from Merck India. Ponceau 4R and Alizarin Red dye powders with 99% purity were purchased from Merck, India. For all solutions preparations fresh triple distilled water was used.

Synthesis of CuO nanoparticles.

The reported procedure was adopted with mild hydrothermal conditions involving experimentally optimized aqueous pH and temperature settings [50]. Aloe vera plant is skin peeled, sliced (50gm) ground to a fine paste, and added to 50 ml of NaOH solution at pH = 5.0. The slimy solution was filtered and the clear filtrate was used as the nanoparticle stabilizing agent. 1.0mM $Cu(NO_3)_2$ solution was prepared and into 20 ml of this, NaOH solution at pH =5 was added along with 50ml of Aloe vera clear filtrate dropwise with constant stirring maintaining 40^0C as the medium temperature. Vigorous stirring was continued for two hours. Black-colored CuO nanoparticles formed are collected after ultracentrifugation with repeated

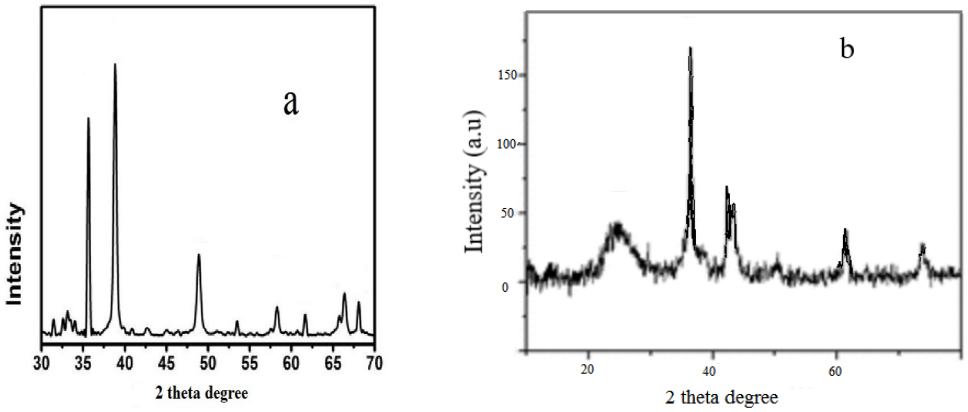

Fig. 2. (a). Powder XRD pattern of CuO nanoparticles and (b). CuO NPs – rGO nanocomposites.

washings. The collected residue was vacuum dried and used for further characterization tests.

Synthesis of rGO

Improved Hummers method was adopted for graphene oxide synthesis from graphite powder [51,52]. Into 1.5g of graphite powder 30ml of 9:1(v/v) mixture of concentrated H_2SO_4 and H_3PO_4 was added along with 9.0g of $KMnO_4$ with constant vigorous stirring for 9 hrs at 50^{0}C. The reaction slurry was cooled to 25^{0}C and 5 ml of 30% (w/v) H_2O_2 was added to convert insoluble MnO_2 into a soluble form. Consequently, excess (250ml) triple distilled water was added and stirred for 2 hrs at 70^0 C · After cooling the rGO residue was washed several times and ultracentrifuged and gathered with ether solvent. Dark brown crystalline GO was vacuum dried and stored for further process. Typically 5 mg of rGO was mixed with 1 mg of CuO NPs and are dispersed in 200 ml of triple distilled water and ultrasonicated for 2 hrs with drop-wise addition of 50ml of 5M NaOH. The black-colored precipitate obtained from this procedure was ultracentrifuged and vacuum dried. The CuO NPs-rGO nanocomposite in as-synthesized forms is subjected to characterization studies.

Characterization technique

The powder XRD of the as-synthesized CuO NPs was taken on Philips PW 1050/37 model instruments operating at 40KV and 30mA. CuKα radiation with 1.54A^0 wavelength and step size of 0.02^0 in 2θ ranges was adopted. HR-TEM of CuO NPs was obtained from CM 20 PHILIPS model, operating at 200KV accelerating voltage instrument respectively. FE-SEM photos are taken on a Hitachi FESEM S4800 microscope. Cyclic voltammetry was performed using a Metrohm Autolab potentiostat/galvanostat PGSTAT-100N with a three-electrode all-glass electrochemical cell fitted with a thermostat and a vent for siphoning out the analyte.

Electrochemical measurement

Glassy Carbon Electrode GCE (2mm dia) modified with CuO NPs–rGO serves as the working electrode, Ag/AgCl, saturated KCl, and platinum wire served as the reference and auxiliary electrodes respectively and potentials are given relative to the reference electrode. CuO NPs–rGO modified GCE was prepared by the drop cast method. The GCE (2mm dia) was polished with alumina slurry 0.5 – 0.05 μm and washed repeatedly with water and finally with ethanol. 3 mg of CuO NPs–rGO was dispersed in 1.0ml of 25% glutaraldehyde as a binder and ultrasonicated the mixture for 30 mins at 25^0 C. The same was drop cast on the GCE disk and allowed to dry under ambient conditions for 10 hrs. In all CV measurements, 0.1M KCl was used as the supporting electrolyte.

RESULTS AND DISCUSSION

Fig. 2(a) shows the powder XRD patterns of CuO NPs. The pattern agrees with the standard JCPDS data file 48-1548 [53]. Applying the Scherrer formula the nano size of the CuO NPs is determined to fall within 15± 2 nm [54]. In Fig. 2(b) the powder XRD of the same CuO- NPs embedded into rGO resulting in CuO NPs-rGO nano compositions is shown. The major sharp-edged peaks in Fig 2(a) are ascribed to (110), (111), (200), (-202), (020), (202), and (113) of pure CuO nanocrystallites. Due to the

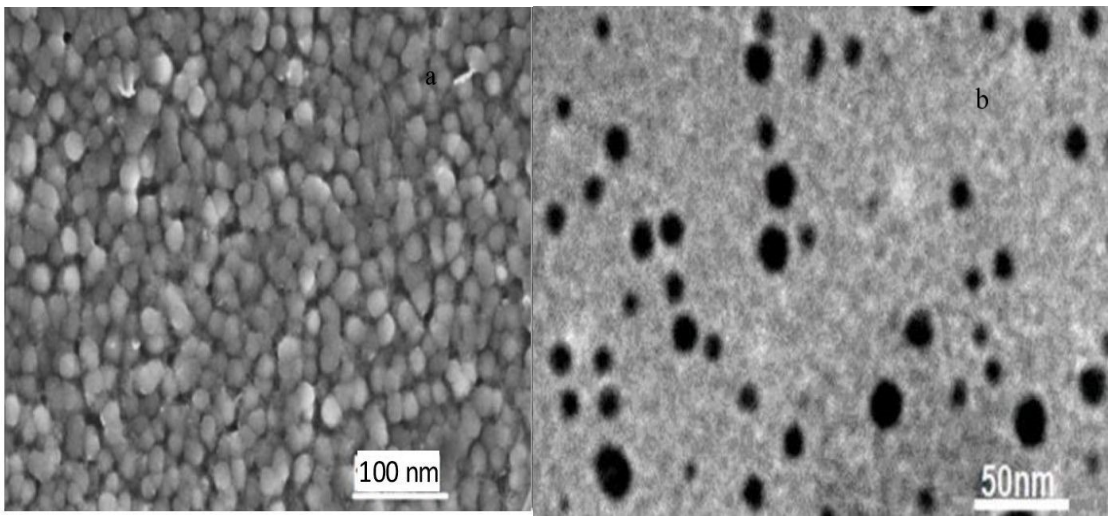

Fig. 3(a). FE – SEM photos and (b).HR – TEM photos of CuO nanoparticles.

presence of carbonaceous matrix in Fig. 2(b), the broad diffraction peak present at 23.8^0 corresponds to the rGO matrix and confirms that rGO is found along with those of CuO- NPs in the powder XRD of nanocomposites.

Also, the diffraction peak of rGO corresponds to an interlayer distance of 0.37nm. In Fig. 2(b), the XRD patterns found are not smooth and may be attributed to the minor variation caused in rGO sheet structures by the implanted metal oxide nanoparticles in the overall sheet-like composite formation [28]. In Fig. 3(a) the SEM and TEM photos of pure CuO NPs are given. Spherical nanoparticles of CuO are being formed when aloe vera plant extract was used as the stabilizing agent in the green synthesis. The average particles size is 15 ± 2nm, which seems agreeable with that of the size value determined from powder XRD results. In Fig. 3(b) SEM and TEM photos of the as-obtained nanocomposites are given. The rGO sheets appear as almost transparent and display flake-like structures on which the CuO NPs are depicted as dark spots. There exists a sharp contrast between rGO sheet and the embedded CuO–NPs. The nanoparticles stand well dispersed without much clogging. Altogether both the SEM and TEM results confirm the decoration of CuO NPs onto 2D- rGO sheet surfaces and the successful formation of nanocomposite structures. In the nanocomposite structure, the particles size of CuO NPs is found to be slightly higher than the pure form which may be due to interactive effects of the rGO surface [55].

In order to investigate the efficiency of CuO NPs–rGO nanocomposites, modified GCE for the enhanced electroactive surface area availability of the electrode, a comparison study was made about the electrode active area of bare GCE by recording cyclic voltammetry in 1.0 mM potassium ferrocyanide electrolyte solution as the model compound having the D_{coff} value as $7.6 cm^2 sec^{-1}$. The supporting electrolyte is 0.2 M KCl applying Randles sevicik [56,57]equation $l_{pa}=2.69*10^5 N^{3/2} AD^{1/2} C\ \nu^{1/2}$ where i_p refers to anodic peak current (μA), n is the number of electrons, A is the electrode surface area (cm^2), D is the diffusion coefficient ($cm^2 s^{-1}$), ν is the scan rate (Vs^{-1}) and C is the concentration(mol. cm^{-3}). By doing so, the electroactive area for plain GCE and CuO-rGO/GCE correspond to 1.99×10^{-3} cm^2 and 2.93×10^{-2} cm^2 respectively. These results infer that CuO-rGO coating on GCE resulted in an appreciable increase in the active surface area nearly 12 times higher compared to unmodified GCE.

Electrooxidations

In Fig. 4. cyclic voltammetry recorded for 2 mM of the two dye solutions at neutral pH in 0.1 KCl are given. In Fig. 4(a) Ponceau 4R dye detection is well seen from the oxidation peaks at different scan rates as 0.45 V. The nanocomposite modified GCE senses the presence of the dye through electro-oxidation occurring at much lower range potentials. The CV scans when proceeded with the positive potentials range the oxidation peak occurs afterward. The reversal to the negative potential region shows that the reduction peak was shifted

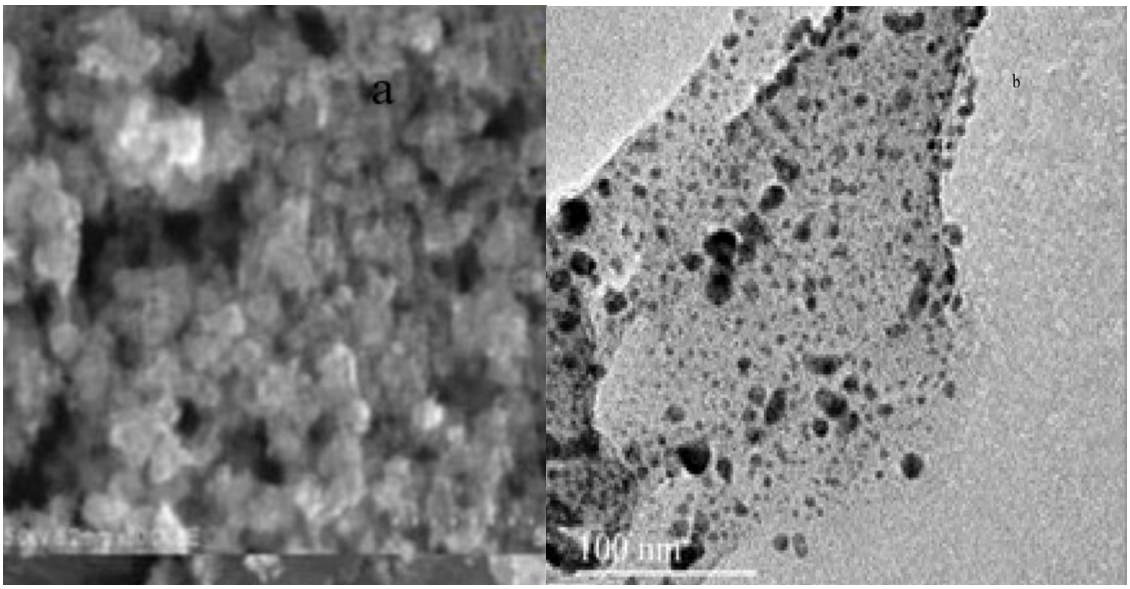

Fig. 4. (a). FE – SEM photos and (b). HR – TEM photos of CuO – rGO nanocomposites.

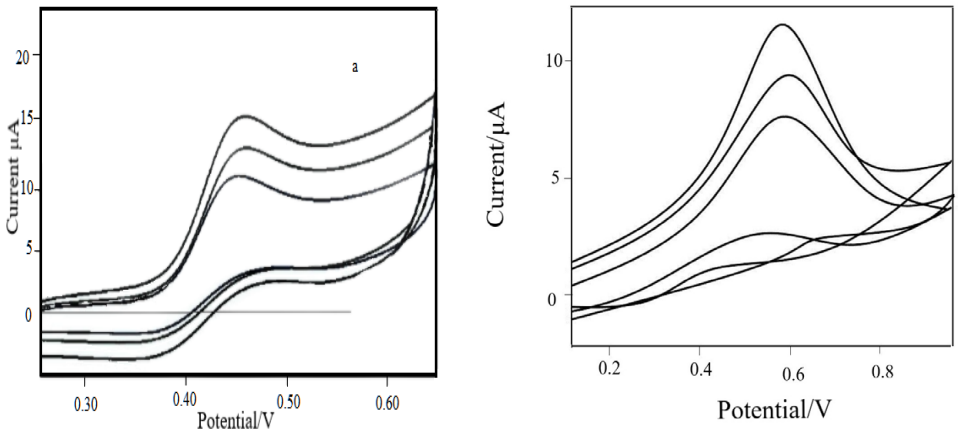

Fig. 5.a. Cyclic voltammogram recorded on CuO NPs – rGO / GCE electrode Vs Ag/AgCl, Sat KCl in presence of 0.1M KCl at scan rates 20, 50, 100 m Vs $^{-1}$, at 25°C for 2.0 m M Ponceau 4R dye and (b). Alizarin red dye

and an irreversible process was detected. Hence the first stage of electron transfer is the oxidation of the dye occurring at 0.45 V. Upon increasing the scan, the voltammogram shows irreversibility regarding the position of the reduced peak. The oxidation peaks are recorded at various scan rates showing the simultaneous increase in the peak current as well. Likewise in Fig. 4(b) the alizarin red dye detection and oxidation peak occurs at 0.6 V. Both the dyes are sensed at lower oxidation potentials by the fabricated GCE. It is noteworthy here to state that the comparison of electrocatalytic oxidations of GCE coated with pure rGO to that of the GCE coated with CuO NPs–rGO nanocomposite, dye degradations produce certain salient features as follows. Although both the chosen dye systems are electro oxidized on the GCE – rGO electrode surface the rate of the dye oxidations are slow, incomplete (only 32% complete) with low% mineralizations, and requiring high oxidation potentials. Nanocompositisation of rGO surface with CuO nanoparticles and when coated onto GCE brought down the dye electro oxidations at a much lower oxidation potential implying an energy-saving process. Also, there is a remarkable increase in the rate of dye degradations for both

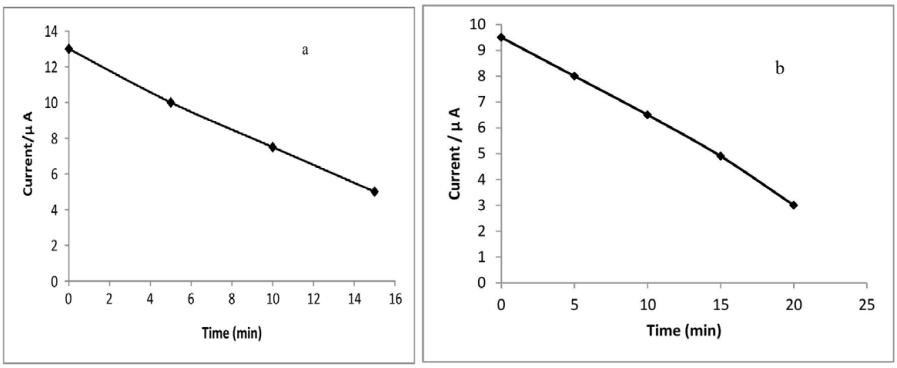

Fig. 6(a). Plots of I_{pa} Vs Time for 2.0 mM solution of Ponceau 4R dye at 20 mVs^{-1} scan rate at 25°C and (b). Alizarin red dye.

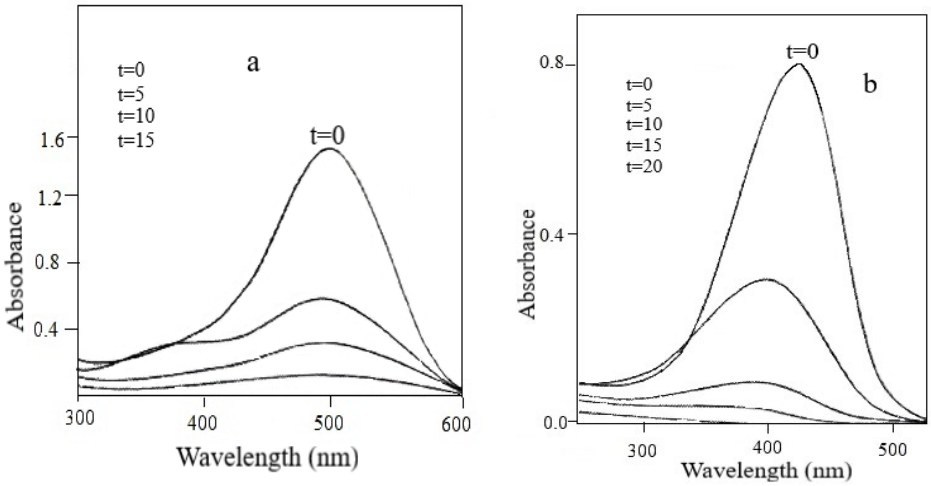

Fig. 7.a. Visible spectra of the Ponceau 4R dye solution drawn out at intervals of time from the electrochemical cell during the electro-oxidation process and (b) Alizarin red dye [DYE] = 2 mM.

P4R and AR dye systems.

Controlled potential electrolysis of the dye solutions is carried out separately at 0.5 V and 0.65 V for P4R and AR respectively. The progress of the oxidative electrolysis was monitored by cyclic voltammetry at a constant scan rate of 50mVs^{-1}.In Fig.6. the peak currents I_{pa} at various time intervals of the dye analyte solution of the two dyes are given separately. It is found that P4R dye degraded in a shorter period compared to AR. The electro oxidations are visible from the decoloration of the dyes. During the electro-oxidation small aliquots are siphoned out and the absorbance spectrum in the visible region is recorded. In Figs. 7 (a) and (b) the visible spectra of the dyes recorded at various intervals of time for P4R and AR are shown.

The absorbance variance with time plots drawn from the spectral data is shown in Fig.8.(a) and (b) for the dye systems. The completion of the dye oxidations is known from the absorbance dropping to near-zero values.

From the absorbance versus time plots data, kinetic plots for first and second-order rate constants are drawn and found that the best fit linear plots existed for first-order oxidation reactions only. From the kinetic plots Fig.9(a) and (b). the rate coefficient values are found for the 2 dyes separately and are given in Table 1. The data indicated that the oxidation of P4R dye occurs faster than the AR dye and the GCE modified with CuO-rGO nanocomposites exhibited efficient sensing activity and surface oxidation activity as well. After the completion of the electrolysis, % mineralization of the dye was determined, and found that P4R dye produced high extent of mineralization than the AR dye system.

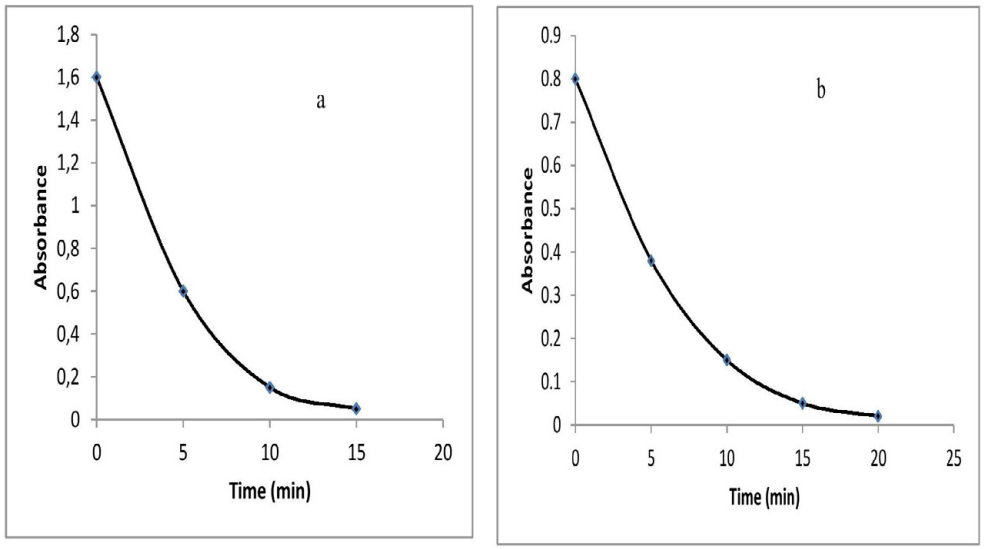

Fig. 8. (a). Absorbance - Time plots for Ponceau 4R and (b). Alizarin red.

Table 1. The overall pseudo-first-order rate coefficient (kx10^{-4} sec^{-1}) values for the oxidation reactions of Ponceau 4R and Alizarin Red using CuO NPs–rGO nanocomposites at 25°C.

Substrate	k	% mineralisation
Ponceau 4 R	1.87	95.7
Alizarin Red	2.90	90.2

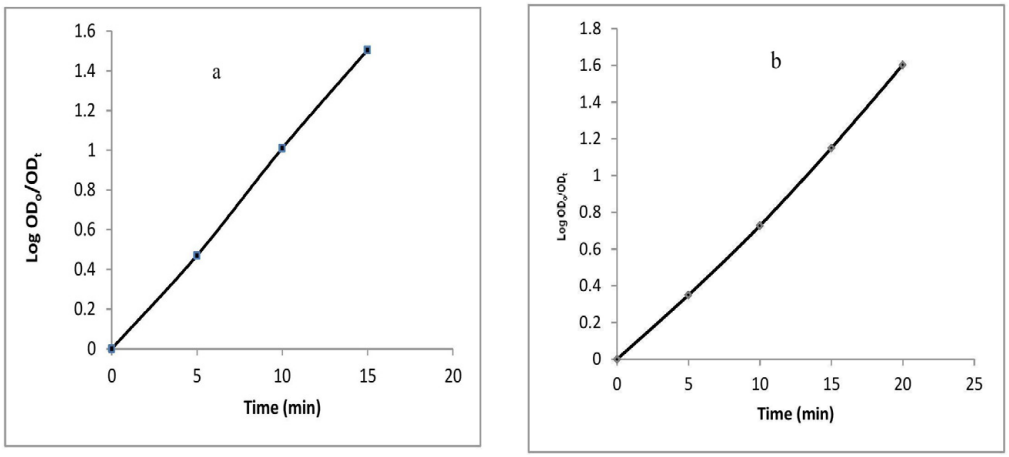

Fig. 9.a. First-order kinetic plots for rate coefficient determination for the electrooxidation of the dye Ponceau 4R and (b) Alizarin red.

In Fig.10, the plausible oxidation mechanism for the two dyes initiated at the electrodic surface is shown. Coating of metal oxide impregnated nanocomposites exhibits enhanced and facile electron transfers from the dye molecules to the oxygenated electrode surface. The presence of an extensive $\pi - \pi^*$ conjugated system of the graphene matrix, facilitates the environment for electrodic electron abduction. Eventually, this step behaves as the rate-determining step because of the electroactive dye molecules undergoing cascades disintegration. These steps are visible by the decoloration of the colored dye analytes. Also due to the presence of anthraquinone functionality in AR, electron abduction from the dye molecule is not easier as in the case of P4R. This aspect is reflected in the increase in the oxidation potential and lower rate coefficient values for AR degradations. In

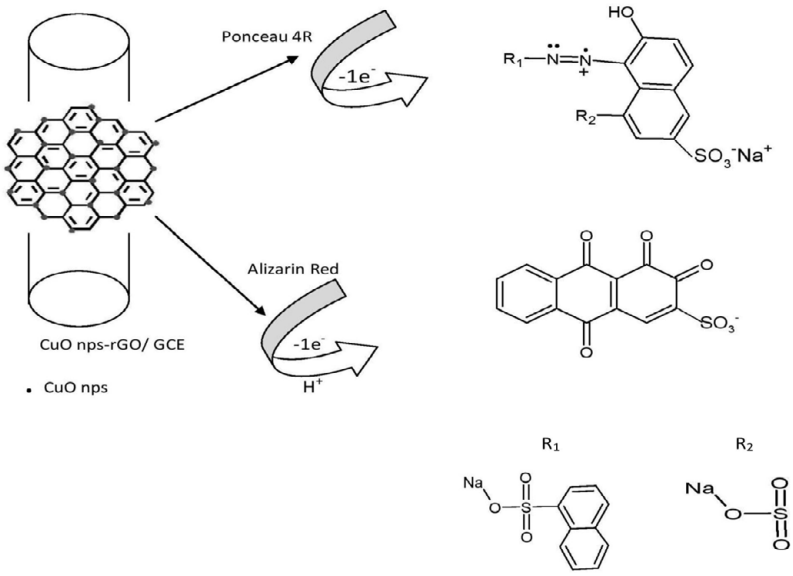

Fig. 10. Plausible oxidation mechanism of (a) Ponceau 4R and (b) Alizarin red dye using CuO NPs–rGO/GCE electrode.

the case of the P4R dye molecule, the presence of azo functional group (-N=N-) renders electron polarization facile and an electrodic electron abduction results in a radically tagged active azo group followed by rapid dye degradation and a higher rate coefficient value. Also, higher % mineralization was detected. Electro activation of anthraquinone nucleus in AR molecule is not facile due to its stability and this results in slower AR degradations and lower % mineralization.

CONCLUSIONS

CuO NPs prepared in a greener route using Aloe vera plant extract as the stabilizing agent could be effectively deposited on to rGO matrix and this resulted in robust hybrid nanocomposite scaffolds that bind conveniently and favorably onto the bare GCE. This modification of GCE provided a large surface area to mass ratio value for the active electrode surface. Metal oxide surface binding onto rGO, brings in, facile electron transfers due to π-π^* conjugations of rGO matrix thereby lowering oxidation potentials considerably. Both the dye systems P4R and AR suffered electro oxidative degradations easily on the modified GCE. Similar results are obtained from the kinetic studies derived from visible spectral absorbance variations with time during the progress of the oxidation of the dyes. Also, the fabricated CuO NPs–rGO nanocomposites coated GCE, proved to possess benign electro-oxidation surface for both dye chosen systems. The prevailing electro catalysis followed in this work on the dye solutions reveals that P4R dye molecules are degraded one and a half times more than compared to AR molecular degradation. This implies that azo groups are easily susceptible to enhanced electro-oxidation than anthraquinone group dyes. No doubt, electrochemical oxidations still prove to be the efficient pathway for cleaning up the dye polluted water sources when appropriately coated electrodic surface and analyte conditions of the industrial wastewater of the dyes are utilized in a combined way.

ACKNOWLEDGEMENTS

The authors thank National Centre for Nano Science and Technology, University of Madras, for the electron microscope photo images of the nanomaterials.

CONFLICTS OF INTEREST

The authors declare that there are no conflicts of interest regarding the publication of this paper.

REFERENCES

1. Mehmood, Rehman, Wang, Farooq, Mahmood, Jadoon, et al. Treatment of Pulp and Paper Industrial Effluent Using Physicochemical Process for Recycling. Water. 2019;11(11):2393.
2. Rajamanickam D, Shanthi M. Photocatalytic degradation of

an organic pollutant by zinc oxide – solar process. Arabian Journal of Chemistry. 2016;9:S1858-S68.
3. Wang JL, Xu LJ. Advanced Oxidation Processes for Wastewater Treatment: Formation of Hydroxyl Radical and Application. Critical Reviews in Environmental Science and Technology. 2012;42(3):251-325.
4. Singh P, Yadav SK, Kuddus M. Green Nanomaterials for Wastewater Treatment. Green Nanomaterials: Springer Singapore; 2020. p. 227-42.
5. Cheriyamundath S, Vavilala SL. Nanotechnology-based wastewater treatment. Water and Environment Journal. 2020;35(1):123-32.
6. Xu P, Zeng GM, Huang DL, Feng CL, Hu S, Zhao MH, et al. Use of iron oxide nanomaterials in wastewater treatment: A review. Science of The Total Environment. 2012;424:1-10.
7. Yaqoob AA, Parveen T, Umar K, Mohamad Ibrahim MN. Role of Nanomaterials in the Treatment of Wastewater: A Review. Water. 2020;12(2):495.
8. Menon S, Agarwal H, Shanmugam VK. Catalytical degradation of industrial dyes using biosynthesized selenium nanoparticles and evaluating its antimicrobial activities. Sustainable Environment Research. 2021;31(1).
9. Hassanien R, Abed-Elmageed AAI, Husein DZ. Eco-Friendly Approach to Synthesize Selenium Nanoparticles: Photocatalytic Degradation of Sunset Yellow Azo Dye and Anticancer Activity. ChemistrySelect. 2019;4(31):9018-26.
10. Angamuthu A, Venkidusamy K, Muthuswami RR. Synthesis and Characterization of Nano-selenium and its Antibacterial Response on Some Important Human Pathogens. Current Science. 2019;116(2):285.
11. Fathima JB, Pugazhendhi A, Oves M, Venis R. Synthesis of eco-friendly copper nanoparticles for augmentation of catalytic degradation of organic dyes. Journal of Molecular Liquids. 2018;260:1-8.
12. Essawy AA. Silver imprinted zinc oxide nanoparticles: Green synthetic approach, characterization and efficient sunlight-induced photocatalytic water detoxification. Journal of Cleaner Production. 2018;183:1011-20.
13. Vissers C, Ming G-l, Song H. Nanoparticle technology and stem cell therapy team up against neurodegenerative disorders. Advanced Drug Delivery Reviews. 2019;148:239-51.
14. Viswanathan A, Rangasamy J, Biswas R. Functionalized Antibacterial Nanoparticles for Controlling Biofilm and Intracellular Infections. Surface Modification of Nanoparticles for Targeted Drug Delivery: Springer International Publishing; 2019. p. 183-206.
15. Wang L, Hu C, Shao L. The antimicrobial activity of nanoparticles: present situation and prospects for the future. International Journal of Nanomedicine. 2017;Volume 12:1227-49.
16. Wang M, Zhang T, Hu Y, Qin Y, Wei W. In Situ Synthesis of Dicarboxylic Acid Functionalized Upconversion Nanoparticles for Bioimaging Applications. ChemPhotoChem. 2018;3(3):145-50.
17. Wang S, Li J, Zhou Z, Zhou S, Hu Z. Micro-/Nano-Scales Direct Cell Behavior on Biomaterial Surfaces. Molecules. 2018;24(1):75.
18. Wang Y, Xu C, Chang Y, Zhao L, Zhang K, Zhao Y, et al. Ultrasmall Superparamagnetic Iron Oxide Nanoparticle for T2-Weighted Magnetic Resonance Imaging. ACS Applied Materials & Interfaces. 2017;9(34):28959-66.
19. Xue Z, Zhang Y, Yu W, Zhang J, Wang J, Wan F, et al. Recent advances in aflatoxin B1 detection based on nanotechnology and nanomaterials-A review. Analytica Chimica Acta. 2019;1069:1-27.
20. Yaqoob AA, Umar K, Ibrahim MNM. Silver nanoparticles: various methods of synthesis, size affecting factors and their potential applications–a review. Applied Nanoscience. 2020;10(5):1369-78.
21. Yaqoob, A. A., Khan, R. M. R., and Saddique, A, Review article on applications and classification of gold nanoparticles. Int. J. Res, 2019; 6 : 762–768.
22. Zhu C, Ahmed I, Parsons A, Liu J, Liu X. The mechanical property, degradation and cytocompatibility analysis of novel phosphate glass fiber textiles. Textile Research Journal. 2018;89(16):3280-90.
23. Yang C, You X, Cheng J, Zheng H, Chen Y. A novel visible-light-driven In-based MOF/graphene oxide composite photocatalyst with enhanced photocatalytic activity toward the degradation of amoxicillin. Applied Catalysis B: Environmental. 2017;200:673-80.
24. Huang M, Feng M, Li H, Huang P, Su Q, Zhang F, et al. Rapid microwave-assisted synthesis of SnO2 quantum dots/reduced graphene oxide composite with its application in lithium-ion battery. Materials Letters. 2017;209:260-3.
25. Naderi HR, Sobhani-Nasab A, Rahimi-Nasrabadi M, Ganjali MR. Decoration of nitrogen-doped reduced graphene oxide with cobalt tungstate nanoparticles for use in high-performance supercapacitors. Applied Surface Science. 2017;423:1025-34.
26. Wang F, Li G, Zhou Q, Zheng J, Yang C, Wang Q. One-step hydrothermal synthesis of sandwich-type NiCo 2 S 4 @reduced graphene oxide composite as active electrode material for supercapacitors. Applied Surface Science. 2017;425:180-7.
27. Khan MA, Kumar A, Zhang J, Kumar M. Recent advances and prospects in reduced graphene oxide-based photodetectors. Journal of Materials Chemistry C. 2021;9(26):8129-57.
28. Ganesan K, Jothi VK, Natarajan A, Rajaram A, Ravichandran S, Ramalingam S. Green synthesis of Copper oxide nanoparticles decorated with graphene oxide for anticancer activity and catalytic applications. Arabian Journal of Chemistry. 2020;13(8):6802-14.
29. Bezza FA, Tichapondwa SM, Chirwa EMN. Fabrication of monodispersed copper oxide nanoparticles with potential application as antimicrobial agents. Scientific Reports. 2020;10(1).
30. Chaudhary RG, Sonkusare VN, Bhusari GS, Mondal A, Shaik DPMD, Juneja HD. Microwave-mediated synthesis of spinel CuAl2O4 nanocomposites for enhanced electrochemical and catalytic performance. Research on Chemical Intermediates. 2017;44(3):2039-60.
31. Verma N, Kumar N. Synthesis and Biomedical Applications of Copper Oxide Nanoparticles: An Expanding Horizon. ACS Biomaterials Science & Engineering. 2019;5(3):1170-88.
32. Kumar PPNV, Shameem U, Kollu P, Kalyani RL, Pammi SVN. Green Synthesis of Copper Oxide Nanoparticles Using Aloe vera Leaf Extract and Its Antibacterial Activity Against Fish Bacterial Pathogens. BioNanoScience. 2015;5(3):135-9.
33. Siddiqi KS, Husen A. Current status of plant metabolite-based fabrication of copper/copper oxide nanoparticles and their applications: a review. Biomaterials Research. 2020;24(1).
34. Khatami M, Varma RS, Heydari M, Peydayesh M, Sedighi A,

Agha Askari H, et al. Copper Oxide Nanoparticles Greener Synthesis Using Tea and its Antifungal Efficiency on Fusarium solani. Geomicrobiology Journal. 2019;36(9):777-81.
35. Akhter SMH, Mohammad F, Ahmad S. Terminalia belerica Mediated Green Synthesis of Nanoparticles of Copper, Iron and Zinc Metal Oxides as the Alternate Antibacterial Agents Against some Common Pathogens. BioNanoScience. 2019;9(2):365-72.
36. Sarkar J, Chakraborty N, Chatterjee A, Bhattacharjee A, Dasgupta D, Acharya K. Green Synthesized Copper Oxide Nanoparticles Ameliorate Defence and Antioxidant Enzymes in Lens culinaris. Nanomaterials. 2020;10(2):312.
37. Rezaire A.B, Montazer. M.Photochem Synthesis of Copper oxide nano particles, J.Protobiol. B.Biol. 2017; 176:100-111.
38. Gupta A, Jamatia R, Patil RA, Ma Y-R, Pal AK. Copper Oxide/Reduced Graphene Oxide Nanocomposite-Catalyzed Synthesis of Flavanones and Flavanones with Triazole Hybrid Molecules in One Pot: A Green and Sustainable Approach. ACS Omega. 2018;3(7):7288-99.
39. Pourbeyram S, Bayrami R, Dadkhah H. Green synthesis and characterization of ultrafine copper oxide reduced graphene oxide (CuO/rGO) nanocomposite. Colloids and Surfaces A: Physicochemical and Engineering Aspects. 2017;529:73-9.
40. El-Abeid SE, Ahmed Y, Daròs J-A, Mohamed MA. Reduced Graphene Oxide Nanosheet-Decorated Copper Oxide Nanoparticles: A Potent Antifungal Nanocomposite against Fusarium Root Rot and Wilt Diseases of Tomato and Pepper Plants. Nanomaterials. 2020;10(5):1001.
41. Huang M, Wang Y, Ying S, Wu Z, Liu W, Chen D, et al. Synthesis of Cu2O-Modified Reduced Graphene Oxide for NO2 Sensors. Sensors. 2021;21(6):1958.
42. Gooding JJ. Nanostructuring electrodes with carbon nanotubes: A review on electrochemistry and applications for sensing. Electrochimica Acta. 2005;50(15):3049-60.
43. Thiam A, Brillas E, Centellas F, Cabot PL, Sirés I. Electrochemical reactivity of Ponceau 4R (food additive E124) in different electrolytes and batch cells. Electrochimica Acta. 2015;173:523-33.
44. C.Benhsinat, F.Beyond, A.Wakrim, M.Azzi, A.Tazi. Decolorization and Degradation of Ponceau 4R by the Super –Iron (VI) in an aqueous solution., Journal of Materials and Environmental Sciences, 2017; 8(5): 1668-1675.
45. Yang X, Sun D, Zeng R, Guo L, Wu K. Trace analysis of ponceau 4R based on the signal amplification of copper-based metal-organic framework modified electrode. Journal of Electroanalytical Chemistry. 2017;794:229-34.
46. Yu L, Shi M, Yue X, Qu L. Detection of allura red based on the composite of poly (diallyldimethylammonium chloride) functionalized graphene and nickel nanoparticles modified electrode. Sensors and Actuators B: Chemical. 2016;225:398-404.
47. Sierra-Rosales P, Berríos C, Miranda-Rojas S, Squella JA. Experimental and theoretical insights into the electrooxidation pathway of azo-colorants on glassy carbon electrode. Electrochimica Acta. 2018;290:556-67.
48. P.A.Pushpanjali, J.G.Manjunatha. Electro analysis of sodium alizarin sulfonate at surfactant modified carbon nanotube paste electrode: A Cyclic voltammetric study, Journal of Materials and Environmental Sciences, 2019; 10(10) :939-947.
49. Zhang Y, Zhang X, Lu X, Yang J, Wu K. Multi-wall carbon nanotube film-based electrochemical sensor for rapid detection of Ponceau 4R and Allura Red. Food Chemistry. 2010;122(3):909-13.
50. R.Vijayalakshmi,S.Kanchana and J.Santhanalakshmi, Green synthesis of copper oxide nano particles from aloe vera extract and its catalytic applications in oxidation of 3-indole derivatives : a kinetic study, JETIR, 2021; 8: 5.
51. Marcano D. C, Kosynkin D.V, Berlin J.M, Sinitskii A,Sun Z, Slesarev A,Alemany L.B, Lu, An improved method for the preparation of graphene oxide (GO) is described. ACS Nano, 2010; **4:** 4806–4814.
52. Marcano D.C, Kosynkin D.V, Berlin J.M, Sinitskii A, Sun Z, Slesarev A.S, Alemany L.B,
Lu W, Preparaton of graphene(GO), ACS Nano, 2018; 12: 2078–2078.
53. Ibrahim AM, Munshi GH, Al-Harbi LM. Copper(II) oxide nanocatalyst preparation and characterization: green chemistry route. Bulletin of the National Research Centre. 2018;42(1).
54. Santhanalakshmi J, Parimala L. The copper nanoparticles catalysed reduction of substituted nitrobenzenes: effect of nanoparticle stabilizers. Journal of Nanoparticle Research. 2012;14(9).
55. Sagadevan S, Zaman Chowdhury Z, Johan MRB, Aziz FA, Salleh EM, Hawa A, et al. A one-step facile route synthesis of copper oxide/reduced graphene oxide nanocomposite for supercapacitor applications. Journal of Experimental Nanoscience. 2018;13(1):284-96.
56. A. J. Bard and L. R. Faulkner, Electrochemical Methods, Wiley, New York, 1980.
57. Rajesh K, Santhanalakshmi J. Design and development of graphene intercalated V2O5 nanosheets based electrochemical sensors for effective determination of potentially hazardous 3,5–Dichlorophenol. Materials Chemistry and Physics. 2017;199:497-507.